

# Charmonium Coherent Photoproduction and Hadroproduction with Effects of Quark Gluon Plasma

Wei Shi,<sup>1</sup> Wangmei Zha,<sup>2</sup> and Baoyi Chen<sup>1,3,\*</sup>

<sup>1</sup>*Department of Physics, Tianjin University, Tianjin 300350, China*

<sup>2</sup>*Department of Modern Physics, University of Science and Technology of China, Hefei 230026, China*

<sup>3</sup>*Institut für Theoretische Physik, Goethe-Universität Frankfurt, Max-von-Laue-Str. 1, D-60438 Frankfurt am Main, Germany*

(Dated: December 27, 2017)

We study the charmonium coherent photoproduction and hadroproduction consistently with modifications from both cold and hot nuclear matters. The strong electromagnetic fields from fast moving nucleus interact with the other target nucleus, producing abundant charmonium in the extremely low transverse momentum region  $p_T < 0.1$  GeV/c. This results in significant enhancement of  $J/\psi$  nuclear modification factor in semi-central and peripheral collisions. In the middle  $p_T$  region such as  $p_T < 3 \sim 5$  GeV/c,  $J/\psi$  final yield is dominated by the combination process of single charm and anti-charm quarks moving in the deconfined matter,  $c + \bar{c} \rightarrow J/\psi + g$ . In the higher  $p_T$  region,  $J/\psi$  production are mainly from parton initial hard scatterings at the beginning of nucleus-nucleus collisions and decay of B hadrons. We include all of these production mechanisms and explain the experimental data well in different colliding centralities and transverse momentum regions.

PACS numbers: 25.75.-q, 12.38.Mh, 24.85.+p

With the nuclear collisions at the relativistic heavy ion collisions (RHIC) and the large hadron collider (LHC), there have been a lot of interesting topics about nuclear properties studied in experiments and theories. One of the main goals at RHIC and LHC is to find a deconfined state of nuclear matter, called “quark-gluon plasma” (QGP), which may be produced in the extremely high energy and/or baryon densities with a phase transition [1], and furthermore, extract the transport properties of this QGP [2]. There are also other projects referred to as “non-QGP” physics, concerning about cosmic ray physics and others [3]. As QGP can only be produced in the nucleon collisions in the overlap area of two nuclei, “non-QGP” topics are usually studied in Ultra-peripheral nuclear collisions (UPC) where QGP background is absent.

In order to study the existence of the extremely hot deconfined matter, produced in the early stage of heavy ion collisions,  $J/\psi$  abnormal suppression has been proposed as one of sensitive signals by Matsui and Satz in 1986 [4].  $J/\psi$  suffers relatively weaker dissociation by the hadron gas compared with QGP, due to its large binding energy [5]. With strong color screening effect and parton inelastic scatterings of QGP,  $J/\psi$  production can be significantly suppressed in nucleus-nucleus collisions, which has been observed in many experiments at RHIC and LHC colliding energies in semi-central and central collisions (with impact parameter  $b < 2R_A$ , where  $R_A$  is the nuclear radius) [6–9]. From RHIC to LHC,  $J/\psi$  production is relatively enhanced in the transverse momentum region  $p_T \leq 3 \sim 5$  GeV/c compared with the scale of the pp collisions [8]. This phenomenon has been well explained with charmonium regeneration mechanism: At higher colliding energy, more charm quark pairs can be produced from hard process in hadronic collisions, which enhance the recombination probability of charm and anti-charm quarks inside QGP [10–14]. New  $J/\psi$ s are continuously regenerated during the QGP evolutions. With sufficiently high initial temperature of QGP and abundant number of charm quarks, the primordially produced  $J/\psi$ s are strongly suppressed and therefore regenerated  $J/\psi$ s dominate the final total yields in Pb-Pb collisions at LHC energies [15, 16].

Also, in the relativistic heavy ion collisions, the nuclei with charges move with nearly the speed of light,  $v > 0.99c$  at RHIC and LHC. The strongest magnetic field on earth can be produced, with a magnitude of  $eB \sim 5m_\pi^2$  at RHIC Au-Au and  $70m_\pi^2$  at LHC Pb-Pb collisions [17, 18]. Electromagnetic fields become strongly Lorentz contracted in the longitudinal direction (nuclear accelerating direction, defined as  $z$ -axis) [19]. In semi-central nuclear collisions, both strong electromagnetic fields and the QGP can be produced [17, 20]. In the QGP, there will be interactions between magnetic fields and chiral light quarks at the limit of zero mass  $m_q = 0$  in the deconfined matter. A lot of topics about the magnetic field induced QCD chirality are studied widely, such as chiral magnetic effect [21, 22], chiral magnetic wave [23], chiral vortical effect [24], and chiral electric separation effect [25].

The electromagnetic fields can also interact with the other nucleus ( $\gamma A$  or  $\gamma N$  interactions) or with the electromagnetic fields of the other nucleus ( $\gamma\gamma$  interactions), and produce hadronic final states [19, 26–30]. Fermi first

---

\*Corresponding author: baoyi.chen@tju.edu.cn

proposed that the transverse electromagnetic fields can be approximated as a swarm of equivalent photons, called ‘‘Equivalent Photon Approximation’’ (EPA) [31]. This idea was also extended by Weizsäcker [32] and Williams [33] independently and therefore also called ‘‘Weizsäcker-Williams-Method’’. This allows a simple and straightforward calculations of vector meson photoproduction between the target nucleus and electromagnetic fields [34]. With long range of electromagnetic interactions, a hard equivalent photon from one nucleus may penetrate into the other nucleus and interact with quarks or gluons. Therefore, one goal of this photoproduction is to study the parton densities of a bound nucleon inside the nucleus, such as shadowing effect. The interactions of  $\gamma A$  (or  $\gamma N$ ) and  $\gamma\gamma$  can produce heavy quark pairs  $Q\bar{Q}$ , dileptons  $l\bar{l}$ , and vector mesons  $V = \phi, \rho^0, J/\psi, \psi(2S)$  [35–38]. In semi-central collisions with  $b < 2R_A$ , these heavy quarks or vector mesons will also go through hot medium and suffer dissociations [39]. With the strong electromagnetic fields, charmonium photoproduction may become larger than the hadroproduction in extremely low  $p_T$  region even in the semi-central collisions with the production of deconfined matter, which has already been observed by experiments at RHIC [40] and LHC [41].

In Pb-Pb semi-central collisions at  $\sqrt{s_{NN}} = 2.76$ , the initial temperature of QGP is around  $(1.5 \sim 2)T_c$  where  $T_c$  is the critical temperature of deconfined phase transition [16]. With the realistic evolutions of QGP and all the sources of charmonium production including photoproduction and hadroproduction (consists of primordial production, regeneration and decay of B hadrons), we give the  $J/\psi$  nuclear modification factor as a function of number of participants  $R_{AA}(N_p)$  and transverse momentum  $R_{AA}(p_T)$ . We find that primordial production, regeneration and photoproduction plays the important role in different  $p_T$  regions of charmonium production, showing different physics on heavy ion collisions.

With a large mass, charmonium evolutions in the hot medium can be described by a classical Boltzmann transport equation. It has described well hadroproduced charmonium  $R_{AA}(N_p)$  at different colliding energies from SPS to LHC [15, 42, 43], mean transverse momentum square  $\langle p_T^2 \rangle(N_p)$  [44], and rapidity distribution  $R_{AA}(y)$  [16]. The transport equation for hadroproduced charmonium with cold and hot nuclear matter effects is

$$\frac{\partial f_\Psi}{\partial \tau} + \mathbf{v}_\Psi \cdot \nabla f_\Psi = -\alpha_\Psi f_\Psi + \beta_\Psi \quad (1)$$

where  $f_\Psi$  is the charmonium distribution in phase space.  $\tau = \sqrt{t^2 - z^2}$  is the local proper time (here  $t$  is the time variable). The second term on the L.H.S. of Eq.(1) represents free streaming of  $\Psi$  with transverse velocity  $\mathbf{v}_T = \mathbf{p}_T / \sqrt{m_\Psi^2 + p_T^2}$ . On the R.H.S. of Eq.(1), the loss term  $\alpha_\Psi$  represents charmonium decay rates in QGP due to color screening effect and parton inelastic scatterings, and is written as

$$\alpha_\Psi = \frac{1}{2E_T} \int \frac{d^3\mathbf{k}}{(2\pi)^3 2E_g} \sigma_{g\Psi}(\mathbf{p}, \mathbf{k}, T) 4F_{g\Psi}(\mathbf{p}, \mathbf{k}) f_g(\mathbf{k}, T) \quad (2)$$

where  $E_g$  and  $E_T = \sqrt{m_\Psi^2 + p_T^2}$  are the gluon energy and charmonium transverse energy, respectively.  $F_{g\Psi}$  is the flux factor. Charmonium decay rate in QGP is proportional to the gluon thermal density  $f_g(\mathbf{k}, T)$  and also their inelastic cross sections  $\sigma_{g\Psi}(T)$  [44]. The cross section for gluon dissociation in vacuum  $\sigma_{g\Psi}(0)$  can be derived through the operator production expansion. It is extended to the finite temperature by geometry scale,  $\sigma_{g\Psi}(T) = \sigma_{g\Psi}(0) \times \langle r_\Psi^2 \rangle(T) / \langle r_\Psi^2 \rangle(0)$ , where  $\langle r_\Psi^2 \rangle(T)$  is the charmonium mean radius square at finite temperature, which can be obtained from potential model with the color screened heavy quark potential from Lattice calculations [45]. The divergence of charmonium radius at  $T \rightarrow T_d^\Psi$  indicates the melting of the bound state  $\Psi$ . Charm and anti-charm quarks in the deconfined matter can also combine to generate a new bound state, represented by the gain term  $\beta_\Psi$ . It is connected with the loss term  $\alpha_\Psi$  through detailed balance between the gluon dissociation process and its inverse process,  $g + \Psi \leftrightarrow c + \bar{c}$ .

With the loss and gain terms in Eq.(1), one can write the analytic solution for charmonium phase space distribution at the time  $\tau$  to be

$$f_\Psi(\mathbf{p}_T, \mathbf{x}_T, \tau | \mathbf{b}) = f_\Psi(\mathbf{p}_T, \mathbf{x}_T - \mathbf{v}_\Psi(\tau - \tau_0), \tau_0) e^{-\int_{\tau_0}^{\tau} d\tau' \alpha_\Psi(\mathbf{p}_T, \mathbf{x}_T - \mathbf{v}_\Psi(\tau - \tau'), \tau')} \\ + \int_{\tau_0}^{\tau} d\tau' \beta_\Psi(\mathbf{p}_T, \mathbf{x}_T - \mathbf{v}_\Psi(\tau - \tau'), \tau') \times e^{-\int_{\tau'}^{\tau} d\tau'' \alpha_\Psi(\mathbf{p}_T, \mathbf{x}_T - \mathbf{v}_\Psi(\tau - \tau''), \tau'')} \quad (3)$$

where  $\tau_0 \sim 0.6 fm/c$  is the time scale of QGP reaching local equilibrium, fixed by light hadron spectra in hydrodynamic models. Charmonium initial distribution in nucleus-nucleus collisions  $f_\Psi(\mathbf{p}_T, \mathbf{x}_T, \tau_0 | \mathbf{b})$  is obtained by the geometry scale with pp collisions  $\hat{f}_\Psi(\mathbf{p}_T, \mathbf{x}_T, \tau_0 | \mathbf{b})$  in Eq.(4), with additional modifications from shadowing effect [46] and Cronin effect [16].

$$\hat{f}_\Psi(\mathbf{p}_T, \mathbf{x}_T, \tau_0 | \mathbf{b}) = \int dz_A dz_B \rho_A(\mathbf{x}_T + \frac{\mathbf{b}}{2}, z_A) \rho_B(\mathbf{x}_T - \frac{\mathbf{b}}{2}, z_B) \frac{d^2 \sigma_{J/\psi}^{pp}}{dy 2\pi p_T dp_T} \quad (4)$$

where  $\rho_{A(B)}$  is the Woods-Saxon nuclear density. The differential cross section for charmonium hadroproduction in pp collisions is parametrized with [16, 47],

$$\frac{d^2\sigma_{J/\psi}^{pp}}{dy2\pi p_T dp_T} = \frac{2(n-1)}{2\pi(n-2)\langle p_T^2 \rangle} \left[ 1 + \frac{p_T^2}{(n-2)\langle p_T^2 \rangle} \right]^{-n} \frac{d\sigma_{J/\psi}^{pp}}{dy} \quad (5)$$

Here  $y = 1/2 \ln[(E + p_z)/(E - p_z)]$  and  $\langle p_T^2 \rangle$  are the rapidity and the mean transverse momentum square of  $J/\psi$ . At  $\sqrt{s_{NN}} = 2.76$  TeV pp collisions, we fit the experimental data of  $J/\psi$  inclusive hadroproduction cross section at forward rapidity  $2.5 < y < 4$  to obtain  $n = 4.0$  and  $\langle p_T^2 \rangle = 7.8$  (GeV/c)<sup>2</sup> [48].  $J/\psi$  rapidity differential cross section is  $d\sigma_{J/\psi}^{pp}/dy = 2.3 \mu\text{b}$  in the forward rapidity [49].

The regeneration rate  $\beta_\Psi$  is proportional to the densities of charm and anti-charm quarks which are produced through nuclear hard process. Charm quark initial densities in nucleus-nucleus collisions are obtained through

$$\rho_c(\mathbf{x}_T, \eta, \tau_0) = \frac{d\sigma_{c\bar{c}}^{pp}}{d\eta} \frac{T_A(\mathbf{x}_T + \mathbf{b}/2)T_B(\mathbf{x}_T - \mathbf{b}/2) \cosh(\eta)}{\tau_0} \quad (6)$$

where  $T_{A(B)}(\mathbf{x}_T)$  is the thickness function of nucleus A(B) at the transverse coordinate  $\mathbf{x}_T$ , with the definition  $T(\mathbf{x}_T) = \int dz \rho(\mathbf{x}_T, z)$ .  $\eta = 1/2 \ln[(t+z)/(t-z)]$  is the spatial rapidity. Charm pair production cross section is taken to be  $d\sigma_{c\bar{c}}^{pp}/d\eta = 0.38$  mb in the forward rapidity  $2.5 < y < 4$  of pp collisions at 2.76 TeV [15, 50]. Shadowing effect reduces charm number by 20% in Pb-Pb collisions [46]. Inspired by the fact that D meson elliptic flows are comparable with light hadrons at  $\sqrt{s_{NN}} = 2.76$  TeV Pb-Pb collisions [51, 52], we assume that charm quarks reach kinetic equilibrium at  $\tau_0$ . With the thermal production of charm pairs strongly suppressed by its large mass, evolutions of charm quark density  $\rho_c(\mathbf{x}_T, \eta, \tau)$  in the expanding QGP satisfy the conservation equation,

$$\partial_\mu(\rho_c u^\mu) = 0 \quad (7)$$

where  $u^\mu$  is the four velocity of QGP fluid cells, given by Eq.(8).

The experimental data of charmonium  $R_{AA}$  also includes the contribution from B hadron decay (called ‘‘non-prompt’’  $J/\psi$ ), with a fraction of  $f_B = N_{B \rightarrow J/\psi}/N_{\text{incl}} = 0.04 + 0.023 p_T / (\text{GeV}/c)$  in the final inclusive yields, depending on the  $p_T$  bins. B hadrons exist as bottom quarks in QGP and suffer energy loss [53–55]. This will change momentum distributions of bottom quark and B hadrons with the total number conservation [56]. One should treat the prompt and non-prompt  $J/\psi$  separately. The prompt  $J/\psi$  cross section is the product of inclusive cross section Eq.(5) and the prompt fraction  $(1 - f_B)$ , and taken as an input in Eq.(4). In the extremely low  $p_T$  region of  $p_T < 0.1$  GeV/c, the fraction of non-prompt  $J/\psi$  drops to only around 0.04. In a certain  $p_T$  window, this non-prompt yield can be enhanced/suppressed due to bottom quark energy loss in QGP, which changes  $J/\psi$  inclusive  $R_{AA}$  in Eq.(23) and will be discussed in details below.

The quark gluon plasma produced at RHIC and LHC turns out to be a strong coupling system. Its evolution can be simulated with (2+1) dimensional ideal hydrodynamic equations, with the assumption of Bjorken expansion in the longitudinal direction,

$$\partial_\mu T^{\mu\nu} = 0 \quad (8)$$

where  $T^{\mu\nu} = (e + p)u^\mu u^\nu - g^{\mu\nu}p$  is the energy-momentum tensor,  $e$  and  $p$  are the energy density and pressure. We also need the equation of state to solve above equations. The deconfined matter is taken to be an ideal gas of massless gluons,  $u$  and  $d$  quarks, and strange quark with mass  $m_s = 150$  MeV [57]. Hadron gas is taken to be an ideal gas of all known hadrons and resonances with mass up to 2 GeV [58]. Two phases are connected with first-order phase transition. With the initial energy density of QGP fixed by the charged hadron multiplicity from experiments, we give the initial maximum temperature of QGP in Table.I. Both local temperature  $T(\mathbf{x}_T, \tau)$  and four velocity  $u^\mu(\mathbf{x}_T, \tau)$  of QGP depend on the coordinate  $\mathbf{x}_T$  and the time  $\tau$ .

Experimental data about  $J/\psi$  production shows significant enhancement in the extremely low  $p_T$  region at  $N_p < 100$  [41], which is attributed to additional photoproduction by the interactions between strong electromagnetic fields from one nucleus and the other target nucleus. In table I, one can see that even at the region of  $N_p < 120$ , QGP initial temperature can still be  $(1.5 \sim 2)T_c$ . Therefore, it is necessary to consider seriously both charmonium hadroproduction and photoproduction and also modifications from hot medium effects at the same time, to reach a full consistent conclusion.

As discussed before, we employ the Equivalent Photon Approximation and treat the transverse electromagnetic fields as a swarm of quasi-real photons in the longitudinal direction. The photons fluctuate into a quark-antiquark pair which then scatter with the target nucleus, mediated by two gluons in the lowest order, but without the net color exchange. It is not clear whether the electromagnetic fields are from the entire source nucleus or spectators, and interact with the entire target nucleus or target spectators at the time of nuclear collisions with

TABLE I: Information of QGP based on (2+1) dimensional ideal hydrodynamics.  $b$  and  $N_p$  are the impact parameter and number of participants.  $T_0^{\text{QGP}}$  and  $\tau_f^{\text{QGP}}$  are the initial maximum temperature and lifetime of QGP.  $T_c$  is the critical temperature of deconfined phase transition.

Hydro in LHC $\sqrt{s_{NN}}=2.76$ TeV Pb-Pb, $2.5 < y < 4$			
b(fm)	$N_p$	$T_0^{\text{QGP}}/T_c$	$\tau_f^{\text{QGP}}$ (fm/c)
0	406	2.6	7.3
9	124	2.1	4.2
10.2	83	1.95	3.5
12	35	1.5	2.3

$b < 2R_A$  [59, 60]. We assume that the interactions between electromagnetic fields and target nucleus happen before hadronic collisions, and therefore the photoproduction do not consider the effects of nucleus broken process. In UPCs, the rapidity differential cross section of  $J/\psi$  exclusive photoproduction has been well studied [27, 61],

$$\frac{d\sigma_{AA \rightarrow AA J/\psi}}{dy}(y) = \frac{dN_\gamma}{dy}(y)\sigma_{\gamma A \rightarrow A J/\psi}(y) + \frac{dN_\gamma}{dy}(-y)\sigma_{\gamma A \rightarrow A J/\psi}(-y) \quad (9)$$

where  $y$  is the rapidity of photoproduced vector mesons (in this case,  $J/\psi$ ). The presence of two terms in Eq.(9) indicates that the colliding nucleus can serve either as a source of electromagnetic fields or as a target. The rapidity of photoproduced  $J/\psi$  is connected with photon energy as  $y = \ln[2w/M_{J/\psi}]$  in laboratory reference frame,  $M_{J/\psi}$  is the  $J/\psi$  mass. Write the photon spectrum as a function of photon energy  $w$ ,  $dN_\gamma/dy = w \cdot dN_\gamma/dw$  with the relation of  $dw/dy = w$ . Now we extend the situation to all centralities with impact parameter dependence. In a certain centrality bin with  $b_{min} \sim b_{max}$ , the photon spectrum becomes [35],

$$n_\gamma(w) = \int_{b_{min}}^{b_{max}} 2\pi b db n_\gamma(w, b) \quad (10)$$

$$n_\gamma(w, b) = \frac{1}{\pi R_A^2} \int_0^{R_A} r dr \int_0^{2\pi} d\phi \frac{d^3 N_\gamma(w, b + r \cos(\phi))}{dw dr d\phi} \quad (11)$$

Since photons interact with the target nucleus coherently to produce vector mesons, the electromagnetic field strength is averaged over the surface of target nucleus with the area  $\pi R_A^2$ .

With the photon-nucleus cross section and photon density, we write  $J/\psi$  coherent photoproduction as a function of rapidity in AA collisions with impact parameter  $b$  to be,

$$\frac{dN_{J/\psi}}{dy}(y|b) = w n_\gamma(w, b) \sigma_{\gamma A \rightarrow J/\psi A}(w) + (y \rightarrow -y) \quad (12)$$

As photons interact with the target coherently, one can not determine the positions of photoproduced  $J/\psi$ s exactly. In order to consider the modifications of anisotropic QGP on photoproduced mesons, we need the spatial distributions of photoproduced  $J/\psi$ s.  $J/\psi$ s are mainly produced by Pomeron exchange process, we distribute the photoproduced  $J/\psi$ s over the nucleus surface with a normalized distribution  $f^{norm}(\mathbf{x}_T)$  proportional to the square of target thickness function  $\sim T_A^2(\mathbf{x}_T)$ . The other limit where photoproduced  $J/\psi$ s are *uniformly* distributed over the target nuclear surface will be discussed below, to check the effects of this distribution uncertainties on the final results.

Now we supplement QGP modifications on photoproduced charmonium,

$$\begin{aligned} \frac{d\tilde{N}_{J/\psi}}{dy}(y|b) = & \int d^2 \mathbf{x}_T w n_\gamma(w, b) \sigma_{\gamma A \rightarrow J/\psi A}(w) \times f^{norm}(\mathbf{x}_T + \mathbf{b}/2) \times [\mathcal{R}_g(\mathbf{x}_T + \mathbf{b}/2, x, \mu)]^2 \times e^{-\int_{\tau_0}^{\tau_f} d\tau \alpha_\Psi(\mathbf{x}_T, \mathbf{b}, \tau)} \\ & + (y \rightarrow -y, \mathbf{b}/2 \rightarrow -\mathbf{b}/2) \end{aligned} \quad (13)$$

where  $\tau_f$  is the lifetime of QGP. We set the origin of coordinates at the middle of the centers of nuclei, and two nuclear centers locate at the positions of  $(0, \pm b/2)$  respectively in transverse plane.  $J/\psi$  decay rate in hot medium  $\alpha_\Psi$  is given in Eq.(2). Equivalent photon density and photon-nucleus cross section are derived below.

Based on EPA method, we obtain the the photon spectrum by setting the energy flux of the fields equal to the energy flux of equivalent photons through the transverse plane,

$$\int_{-\infty}^{\infty} d\tau \int d\mathbf{x}_T \cdot \mathbf{S} = \int_0^{\infty} dw w n(w) \quad (14)$$

where  $\mathbf{S} = \mathbf{E}_T \times \mathbf{B}_T$  is the Poynting vector and  $n_\gamma(w) \equiv dN_\gamma/dw$  is the photon spectrum. Introducing the impact parameter dependence in photon spectrum, it becomes [62],

$$\begin{aligned} n_\gamma(w, b) &= \frac{1}{\pi w} |\mathbf{E}_T(w, b)|^2 \\ &= \frac{Z^2 \alpha}{4\pi^3 w} \left| \int_0^\infty dk_T k_T^2 \frac{F(k_T^2 + \frac{w^2}{\gamma_L^2})}{k_T^2 + \frac{w^2}{\gamma_L^2}} J_1(bk_T) \right|^2 \end{aligned} \quad (15)$$

where  $Ze$  is the nuclear charge ( $e$  is the magnitude of electron charge). Here we employ the relation of  $|\mathbf{E}_T| \approx |\mathbf{B}_T|$  in the first line in the limit of  $v/c \approx 1$ ,  $v$  is the nucleon velocity. Nucleon Lorentz factor  $\gamma_L = \sqrt{s_{NN}}/(2m_N)$  is at the orders of  $\sim 100$  at RHIC and  $\sim 1000$  at LHC.  $\alpha = e^2/(\hbar c)$  is the electromagnetic coupling constant ( $\hbar = c = 1$  in this work).  $k_T$  is the photon transverse momentum,  $J_1$  is the first kind Bessel function. The nuclear form factor  $F(q^2)$  is the Fourier transform of the charge distribution in nucleus (taken as Woods-Saxon distribution). In the Ultra-peripheral collisions with  $b > 2R_A$ , one can approximate the nucleus as a pointlike particle without inner charge distribution, and still obtain similar electromagnetic fields [39]. With the form factor of a pointlike particle, the photon spectrum Eq.(15) is given analytically,

$$n_\gamma(w, b) = \frac{Z^2 w \alpha}{4\pi^3 \gamma_L^2} \left[ K_1\left(\frac{wb}{\gamma_L}\right) \right]^2 \quad (16)$$

where  $K_1$  is a modified Bessel function. Note that this photon spectrum Eq.(16) for pointlike particle is close to the realistic situation at UPCs, but diverges at small impact parameter  $b < 2R_A$  where nucleus can not be treated as a ‘‘pointlike’’ particle anymore. In this work, we do the realistic calculations with Eq.(15) in all centralities. For the comparison between different form factors, please see Ref.[39].

There is another ingredient we need for the charmonium photoproduction,  $\sigma_{\gamma A \rightarrow J/\psi A}(w)$ , which can be obtained from photon-proton cross sections with optical theorem and Glauber calculations. We write photo-nuclear cross section into a differential form,

$$\sigma_{\gamma A \rightarrow J/\psi A} = \frac{d\sigma_{\gamma A \rightarrow J/\psi A}}{dt} \Big|_{t=0} \int_{-t_{min}}^\infty dt |F(t)|^2 \quad (17)$$

Here  $-t_{min} = [M_{J/\psi}^2/(4w\gamma_L)]^2$  is the minimum momentum transfer squared needed to produce a vector meson of mass  $M_{J/\psi}$  in the laboratory reference frame. Note the nuclear form factor  $F(t)$  is significant only for  $|t| < (1/R_A)^2$ , The differential photo-nuclear cross section is

$$\frac{d\sigma_{\gamma A \rightarrow J/\psi A}}{dt} \Big|_{t=0} = \frac{\alpha \sigma_{tot}^2(J/\psi A)}{4f_V^2} \quad (18)$$

$$\sigma_{tot}(J/\psi A) = \int d^2\mathbf{x}_T [1 - e^{-\sigma_{tot}(J/\psi p)T_A(\mathbf{x}_T)}] \quad (19)$$

where  $f_V^2/4\pi = 10.4$  is determined by  $J/\psi$  mass and its leptonic decay width with a proper modification based on generalized vector dominance model (GVDM) and photoproduction data [63]. Eq.(19) express the  $J/\psi$ -nuclear cross section as a function of  $J/\psi$ -proton cross section by thickness function. Using optical theorem again, and connect the vector meson-proton cross section with the photon-proton cross section measured by HERA, one can obtain

$$\sigma_{tot}^2(J/\psi p) = \frac{4f_V^2}{\alpha} \frac{d\sigma(\gamma p \rightarrow J/\psi p)}{dt} \Big|_{t=0} \quad (20)$$

There are Pomeron and meson exchange portion contributing to the cross section. The meson exchange term falls rapidly as the center of mass energy  $W_{\gamma p}$  increases, it is strongly suppressed in heavy vector meson production such as  $\phi$  and  $J/\psi$ . The cross section may be parametrized with HERA data as [64]

$$\frac{d\sigma(\gamma p \rightarrow J/\psi p)}{dt} \Big|_{t=0} = b_V X W^\epsilon \times \left[ 1 - \left( \frac{M_{J/\psi} + M_p}{W_{\gamma p}} \right)^2 \right] \quad (21)$$

with  $b_V = 4 \text{ GeV}^{-2}$ ,  $X = 0.00406 \mu b$  and  $\epsilon = 0.65$ .  $M_{J/\psi}$  and  $M_p$  are the mass of  $J/\psi$  and proton. The center of mass energy of the scattering particles ( $\gamma$  and  $p$ ) is  $W_{\gamma p} = 2\sqrt{wE_p}$  with  $E_p$  to be the proton energy. For more details about the extraction of  $\gamma p$  cross section, please see [35].

The vector mesons are produced after photon fluctuating into hadronic states through two gluon exchanges with the target nucleus. Therefore, vector meson production is proportional to the square of gluon densities in the target nucleus. With shadowing effect modifications on nuclear gluon distributions at small Bjorken- $x$ , photoproduction of vector mesons can be significantly suppressed especially at LHC energies. For photoproduced vector mesons, the resolution scale in gluon density is chosen as  $\mu^2 = M_{J/\psi}^2/4 \text{ GeV}^2$  [61, 65]. With the relation of  $-t \ll M_{J/\psi}^2$ , the fraction of gluon momentum is around  $x \approx M_{J/\psi}^2/W_{\gamma p}^2 = \frac{M_{J/\psi}}{\sqrt{s_{NN}}}e^{-y}$ , at the order of  $10^{-3} \sim 10^{-5}$  at  $\sqrt{s_{NN}} = 2.76 \text{ TeV}$ .

With charmonium hadroproduction (initial production, regeneration and decay from B hadrons) and photoproduction, now we can write the prompt and inclusive nuclear modification factors,

$$R_{AA}^{\text{prompt}} = \frac{N^{\gamma A \rightarrow J/\psi A} + N_{AA}^{J/\psi}}{N_{pp}^{J/\psi} N_{\text{coll}}} \quad (22)$$

$$R_{AA} = \frac{R_{AA}^{\text{prompt}}}{1 + r_B} + \frac{r_B \times Q}{1 + r_B} \quad (23)$$

where  $N^{\gamma A \rightarrow J/\psi A}$  represents the charmonium photoproduction with hot medium effects in AA collisions. Photoproduction in pp collisions is negligible compared with AA situation.  $N_{AA}^{J/\psi}$  is  $J/\psi$  prompt hadroproduction, obtained from the integration of Eq.(3).  $N_{\text{coll}} = \sigma_{\text{incl}} \int d^2\mathbf{x}_T T_A(\mathbf{x}_T + \mathbf{b}/2) T_B(\mathbf{x}_T - \mathbf{b}/2)$  is the number of binary collisions, with  $\sigma_{\text{incl}}$  to be the inelastic cross section between two nucleons.  $r_B = f_B/(1 - f_B)$  is the ratio of non-prompt over prompt  $J/\psi$  yields in pp collisions. In a certain  $p_T$  window, bottom quark number can be modified by a quench factor  $Q = N_{AA}^b/(N_{\text{coll}} N_{pp}^b)$  in QGP due to the energy loss, which satisfies  $Q \geq 1$  and  $Q \leq 1$  in small and high  $p_T$  regions, respectively [56]. Considering that the fraction of non-prompt  $J/\psi$  is much smaller than the prompt part, it will change  $J/\psi$  inclusive  $R_{AA}$  slightly and is neglected in this work by taking  $Q = 1$ . Note that in the situation where B hadron decay becomes dominant such as  $\psi(2S)$  inclusive yields in Pb-Pb collisions, effects of bottom quark energy loss should be treated seriously [56].

In Ultra-peripheral collisions with  $b > 2R_A$ , there will be no hadroproduction and denominator of Eq.(22) approaches to zero. In the extremely low  $p_T$  regions where photoproduction becomes important, photoproduction becomes non-zero at the limit of  $N_p \rightarrow 0$ , makes  $R_{AA}^{\text{prompt}} \rightarrow \infty$  and  $R_{AA} \rightarrow \infty$ , see both experimental data and our theoretical results below.

Before quantitative calculations, let's analyse the different charmonium production in different  $p_T$  regions. As equivalent photon number decreases with frequency rapidly, photoproduced  $J/\psi$ s mainly distribute at  $p_T < 0.1 \text{ GeV}/c$  with mean transverse momentum  $\langle p_T \rangle_{J/\psi} \approx 0.055 \text{ GeV}/c$  [41]. Beyond this  $p_T$  bin, the hadroproduction becomes important. With strong energy loss of charm quarks, the regenerated  $J/\psi$ s are mainly distributed below  $3 \sim 5 \text{ GeV}/c$ . At higher  $p_T$  bins,  $J/\psi$ s from initial production and decays of B hadrons dominates. Please see Fig.1.

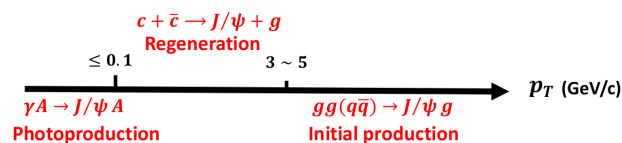


FIG. 1: (Color online) Schematic diagram for different charmonium production mechanisms at different transverse momentum regions in semi-central nucleus-nucleus collisions with the existence of both QGP and strong transverse electromagnetic field. Photoproduction, regeneration and initial production dominates  $J/\psi$  final yields in extremely low  $p_T$ , low and middle  $p_T$ , high  $p_T$  regions, respectively.

Before starting the comparison between charmonium hadroproduction and photoproduction in semi-central collisions with the existence of QGP, we give the charmonium photoproduced cross section as a function of rapidity, which has been well studied in Ultra-peripheral collisions. With the increasing rapidity, it takes more energy  $w$  for quasi-real photons to fluctuate into a  $J/\psi$  with rapidity  $y$ ,  $w \propto e^y$ . Therefore, the cross section in Fig.2 decreases with rapidity. After considering the shadowing effect, both lines in Fig.2 will be shifted downward, with the magnitude depending on different shadowing suppression factors.

Charmonium hadroproduction is proportional to the number of binary collisions  $N_{\text{coll}}$ . With increasing overlap area between two nuclei, the number of binary collisions and participants increase significantly. However, the electromagnetic fields produced by two nuclei increases at first and then decreases with  $N_p$ , which makes photoproduction reach the maximum value at semi-central collisions. In Fig.3, the solid and dotted lines represent

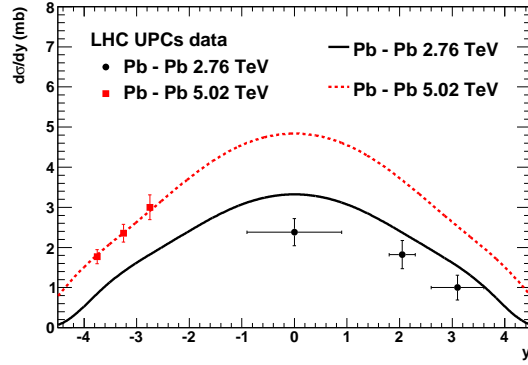


FIG. 2: (Color online)  $J/\psi$  coherent photoproduction as a function of rapidity in Ultra-peripheral collisions at 2.76 TeV and 5.02 TeV Pb-Pb collisions. Theoretical calculations does not include the shadowing effect. Experimental data is from ALICE Collaboration [66–68].

photoproduction and initial hadroproduction scaled from  $pp$  collisions, both without modifications from cold (such as shadowing effect) and hot medium effects. It helps to clarify the relation between two production mechanisms. At around  $N_p > 200$  (with  $b < 7$  fm), the hadroproduction becomes about five times larger than the photoproduction, and the interactions between strong electromagnetic fields and target nucleus seems negligible. With the fact that charmonium from hadronic collisions only distributed in the overlap area of two nuclei where QGP is produced, but coherently photoproduced charmonium is distributed over the entire target nucleus surface, the QGP suppression on photoproduced charmonium should always be weaker than the hadroproduction. At  $N_p$  of  $100 \sim 150$  where QGP initial temperature is  $\sim 2T_c$ , 20%  $\sim$  40% of photoproduced  $J/\psi$ s is dissociated due to parton inelastic collisions and color screening effect.

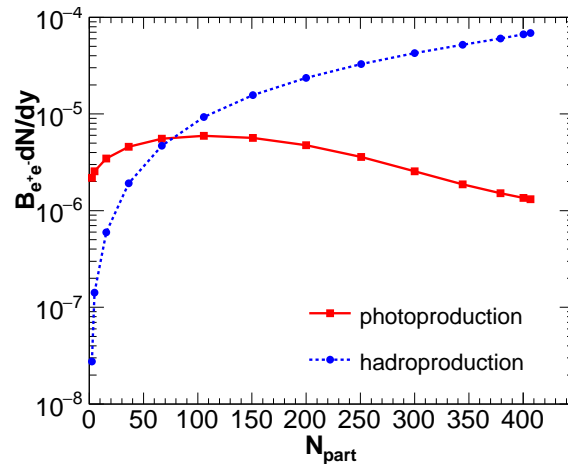


FIG. 3: (Color online) Charmonium hadroproduction scaled from  $pp$  collisions and photoproduction as a function of number of participants  $N_p$  at the forward rapidity  $2.5 < y < 4$  in  $\sqrt{s_{NN}} = 2.76$  Pb-Pb collisions in the extremely low transverse momentum region  $p_T < 0.3$  GeV/c. Both lines are without modifications from shadowing effect and QGP suppression.  $B_{e^+e^-}$  is the branch ratio of  $J/\psi \rightarrow e^+e^-$ .

Coherent photoproduced charmonium is from the quasi-real photon fluctuations into a vector meson, which is different from the parton fusions in hadronic collisions. In Fig.4, we compare the different mechanisms for charmonium production as a function of  $p_T$  with impact parameter  $b=10.2$  fm. The hadroproduction shows a flat behavior in  $p_T < 1$  GeV/c. In the  $p_T < 0.1$  GeV/c where photoproduction becomes non-zero (solid line),  $R_{AA}$  is significantly enhanced and even larger than the unit. With increasing  $p_T$ , charm quark density in QGP decreases as a fermi-distribution (thermalization limit) or power law (given by pQCD), regeneration (dashed line) drops to zero at  $p_T \sim 3$  GeV/c [48]. In higher  $p_T$  bins, final charmonium mainly consists of initial production from parton hard scatterings. The tendency of  $R_{AA}(p_T)$  in Fig.4 is very similar with RHIC data at cent.20-40% [40]. The

enhancement of  $R_{AA}$  in  $p_T < 0.1$  GeV/c will be more significant at larger impact parameter.

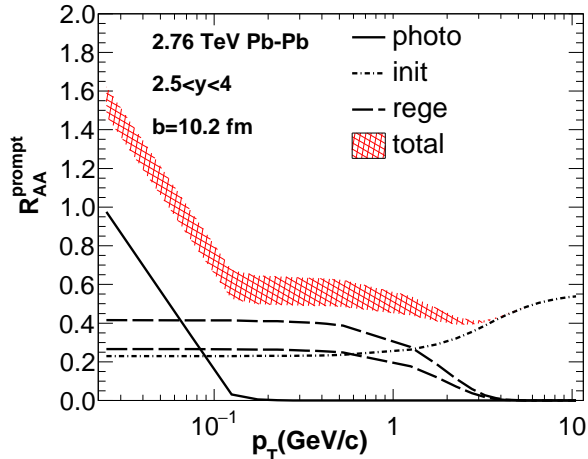


FIG. 4: (Color online) Charmonium *prompt* nuclear modification factor as a function of transverse momentum, at the impact parameter  $b = 10.2$  fm in forward rapidity  $2.5 < y < 4$  at LHC 2.76 TeV Pb-Pb collisions. Dot-dashed line is initial production, dashed lines is the regeneration (two lines represent 20% difference of charm pair production cross section  $d\sigma_{pp}^{c\bar{c}}/dy$  due to its large uncertainties measured by experiments). Solid line is the photoproduction with cold and hot medium modifications. Color band is the total contribution (including initial production, regeneration and photoproduction).

Now we give the nuclear modification factor as a function of centrality. The experimental data in Fig.5-6 is for inclusive  $J/\psi$ , we already include the contribution from B hadron decay in the total production (color band). In the central collisions, the regeneration becomes important due to the abundant number of  $c\bar{c}$  pairs in QGP. In peripheral collisions, both QGP lifetime and charm pair number become smaller, which suppresses the regeneration. The initially produced  $J/\psi$ s suffer weaker suppression in the semi-central and peripheral collisions. Photoproduction from strong electromagnetic fields dominates in the peripheral collisions. The nuclear modification factor  $R_{AA}$  in  $p_T < 0.3$  GeV/c (Fig.5) is much larger than the value in  $p_T > 0.3$  GeV/c (Fig.6) at  $N_p \leq 100$ . This  $R_{AA}$  enhancement in particular  $p_T$  bin is attributed to the photoproduction.

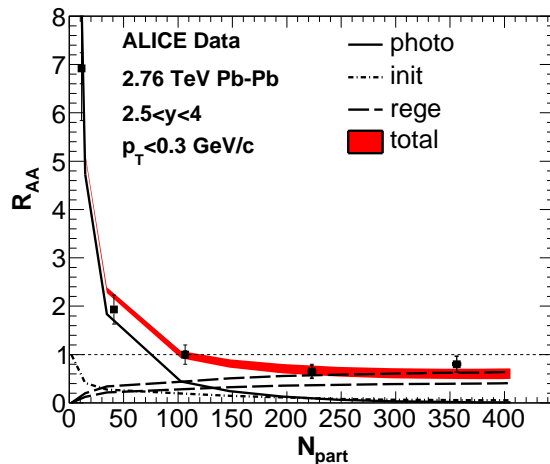


FIG. 5: (Color online) Charmonium *inclusive* nuclear modification factor as a function of number of participants  $N_p$  in  $p_T < 0.3$  GeV/c in forward rapidity  $2.5 < y < 4$  at LHC 2.76 TeV Pb-Pb collisions. (Dot-dashed, dashed, solid) lines are the initial production, regeneration and photoproduction, respectively. Color band is the total production including decay from B hadrons (non-prompt  $J/\psi$ ). Experimental data is from ALICE Collaboration [41].

Finally, let's analyse the uncertainties in our theoretical calculations. The photon-nucleus cross section  $\sigma_{\gamma A \rightarrow J/\psi A}$  depends on the parametrization of  $\gamma p$  differential cross section and charmonium properties [69]. This uncertainty can be partially constrained by the experimental data of charmonium photoproduction in UPCs. One of another important inputs is the charmonium hadronic cross section  $d^2\sigma_{pp}^{J/\psi}/dydp_T$  ( used in the numerator



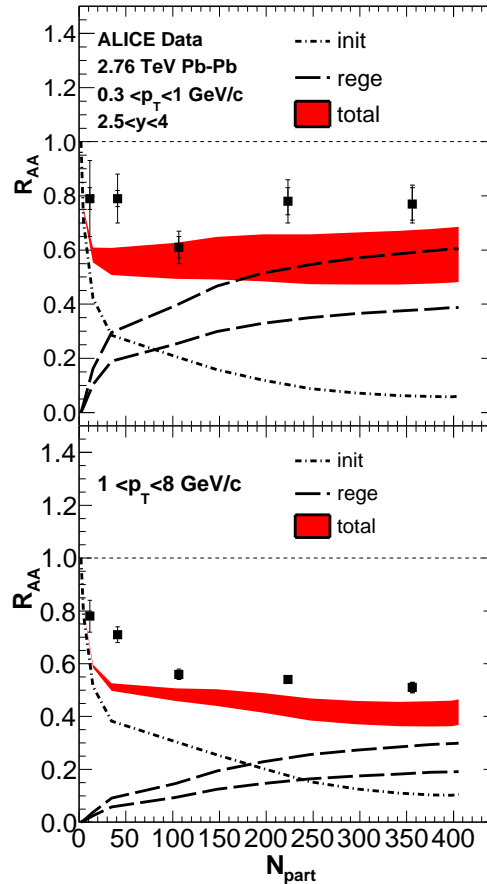


FIG. 6: (Color online) Charmonium *inclusive* nuclear modification factors as a function of number of participants  $N_p$  in  $0.3 < p_T < 1$  and  $1 < p_T < 8$  GeV/c in forward rapidity  $2.5 < y < 4$  at LHC 2.76 TeV Pb-Pb collisions. Lines and color band are the same with Fig.5. The upper limit of color band will be shifted upward if employing a larger charm cross section  $d\sigma_{c\bar{c}}^{pp}/dy$  which is with large uncertainty in experiments [50]. Note that photoproduction in these  $p_T$  regions is negligible and therefore absent in this figure. Experimental data is from ALICE Collaboration [41].

and denominator of  $R_{AA}$ ) in the low  $p_T$  region absent of experimental data. Our parametrization Eq.(5) is very close to the parametrization employed by ALICE Collaboration to obtain experimental  $R_{AA}$ , with the difference of  $p_T$ -dependence less than 4% [70], which ensures the same definitions of our theoretically calculated  $R_{AA}$  and the experimental data. Another uncertainty is the shadowing effect. With EPS09 model, it suppresses gluon distribution by around 20% in the Bjorken- $x$  corresponding to charmonium in forward rapidities. However, different models give very different magnitudes of shadowing effect. In the limit without shadowing effect, both charmonium photoproduction and hadroproduction become  $\sim 1/0.8^2$  times of above results. For the QGP induced  $J/\psi$  decay rate, our values from Eq.(2) is similar with other groups [71]. In order to introduce the spatial distribution of coherently photoproduced  $J/\psi$  over the nuclear surface, we assume the charmonium density to be proportional to the square of gluon densities inspired by the Pomeron exchange process. In the other limit that photoproduced charmonium distribution is proportional to the photon spatial density which changes slowly with the coordinates, we assume a *uniform* charmonium distribution over the nuclear surface. With the fact that shadowing effect becomes weaker in the edge of nucleus, *uniform* distribution suffers weaker shadowing effect and QGP dissociation. These make the final photoproduction  $N^{\gamma A \rightarrow J/\psi A}$  in Eq.(22) increases by around 20% in semi-central collisions.

The incoherently photoproduced  $J/\psi$ s can also contribute to the charmonium  $R_{AA}$ . They are mainly distributed in a larger  $p_T$  region compared with coherent  $J/\psi$ , such as  $0.2 < p_T < 0.8$  GeV/c [66]. In  $p_T < 0.2$  GeV/c, incoherent production is much smaller than the coherent part, and neglected in our calculations. In higher  $p_T$  regions, it becomes the main source for  $J/\psi$  production in Ultra-peripheral collisions. However, in semi-central collisions where hadroproduction increases linearly with  $p_T$  at  $p_T < 1$  GeV/c [48], incoherent photoproduction is also negligible for the  $p_T$ -integrated observables at  $0.3 < p_T < 1$  GeV/c. For the particular  $p_T$  bin, such as

0.1  $\sim$  0.5 GeV/c, the importance of incoherent photoproduction needs detailed studies.

In summary, we employ the Boltzmann-type transport model to study charmonium hadronic production including initial production, regeneration and decay from B hadrons. In extremely low  $p_T$  region, charmonium photoproduction is supplemented with modifications of both shadowing effect and QGP suppressions. In peripheral collisions and extremely small  $p_T$  region, photoproduction becomes larger than the hadroproduction, and is mainly suppressed by shadowing effect with large uncertainties instead of QGP. However, in semi-central collisions, both shadowing effect and QGP suppression becomes important on charmonium production. And around 20%  $\sim$  40% of photoproduced  $J/\psi$ s can be dissociated by QGP at  $100 < N_p < 150$ . In (extremely low, middle, high)  $p_T$  regions, photoproduction, regeneration and initial production play the dominant roles respectively in charmonium final production, which help to clarify *different physics* such as shadowing effect on gluon distribution in small Bjorken- $x$ , charm quark thermalization (controls regeneration), charmonium dissociation by QGP in relativistic heavy ion collisions.

**Acknowledgement:** We thank Guansong Li for helpful discussions. WS and BC are supported by NSFC Grant No. 11705125 and 11547043, BC is also supported by Sino-Germany (CSC-DAAD) Postdoc Scholarship. WZ is supported by NSFC Grant No. 11775213 and 11505180.

- 
- [1] A. Bazavov *et al.*, Phys. Rev. D **85**, 054503 (2012)
  - [2] H. Song and U. W. Heinz, J. Phys. G **36**, 064033 (2009)
  - [3] A. A. Anselm, Phys. Lett. B **217**, 169 (1989).
  - [4] T. Matsui and H. Satz, Phys. Lett. **B178**, 416(1986).
  - [5] H. Satz, J. Phys. G **32**, R25 (2006)
  - [6] A. Adare *et al.* [PHENIX Collaboration], Phys. Rev. Lett. **98**, 232301 (2007)
  - [7] B. I. Abelev *et al.* [STAR Collaboration], Phys. Rev. C **80**, 041902 (2009)
  - [8] B. B. Abelev *et al.* [ALICE Collaboration], Phys. Lett. B **734**, 314 (2014)
  - [9] J. Adam *et al.* [ALICE Collaboration], Phys. Lett. B **766**, 212 (2017)
  - [10] R. L. Thews, M. Schroedter and J. Rafelski, Phys. Rev. C **63**, 054905 (2001)
  - [11] P. Braun-Munzinger and J. Stachel, Phys. Lett. B **490**, 196 (2000)
  - [12] L. Yan, P. Zhuang and N. Xu, Phys. Rev. Lett. **97**, 232301 (2006)
  - [13] A. Andronic, P. Braun-Munzinger, K. Redlich and J. Stachel, Phys. Lett. B **571**, 36 (2003)
  - [14] X. Zhao and R. Rapp, Nucl. Phys. A **859**, 114 (2011)
  - [15] K. Zhou, N. Xu, Z. Xu and P. Zhuang, Phys. Rev. C **89**, no. 5, 054911 (2014)
  - [16] B. Chen, Phys. Rev. C **93**, no. 5, 054905 (2016)
  - [17] W. T. Deng and X. G. Huang, Phys. Rev. C **85**, 044907 (2012)
  - [18] K. Tuchin, Adv. High Energy Phys. **2013**, 490495 (2013)
  - [19] F. Krauss, M. Greiner and G. Soff, Prog. Part. Nucl. Phys. **39**, 503 (1997).
  - [20] C. Shen and U. Heinz, Phys. Rev. C **85**, 054902 (2012) Erratum: [Phys. Rev. C **86**, 049903 (2012)]
  - [21] M. A. Metlitski and A. R. Zhitnitsky, Phys. Rev. D **72**, 045011 (2005)
  - [22] D. E. Kharzeev, L. D. McLerran and H. J. Warringa, Nucl. Phys. A **803**, 227 (2008)
  - [23] Y. Burnier, D. E. Kharzeev, J. Liao and H. U. Yee, Phys. Rev. Lett. **107**, 052303 (2011)
  - [24] D. E. Kharzeev and D. T. Son, Phys. Rev. Lett. **106**, 062301 (2011)
  - [25] X. G. Huang and J. Liao, Phys. Rev. Lett. **110**, no. 23, 232302 (2013)
  - [26] G. Baur, K. Hencken, D. Trautmann, S. Sadovsky and Y. Kharlov, Phys. Rept. **364**, 359 (2002)
  - [27] S. R. Klein and J. Nystrand, Phys. Rev. Lett. **92**, 142003 (2004)
  - [28] C. A. Bertulani, S. R. Klein and J. Nystrand, Ann. Rev. Nucl. Part. Sci. **55**, 271 (2005)
  - [29] G. M. Yu and Y. D. Li, Chin. Phys. Lett. **31**, no. 1, 011202 (2014); G. M. Yu, Y. B. Cai, Y. D. Li and J. S. Wang, Phys. Rev. C **95**, no. 1, 014905 (2017).
  - [30] G. M. Yu, Y. C. Yu, Y. D. Li and J. S. Wang, Nucl. Phys. B **917**, 234 (2017); G. M. Yu and Y. D. Li, Phys. Rev. C **91**, no. 4, 044908 (2015).
  - [31] E. Fermi, Z. Phys. **29**, 315 (1924).
  - [32] C. F. von Weizsacker, Z. Phys. **88**, 612 (1934).
  - [33] E. J. Williams, Proc. Roy. Soc. A **139**, 163 (1933)
  - [34] V. A. Khoze, A. D. Martin and M. G. Ryskin, Eur. Phys. J. C **24**, 459 (2002)
  - [35] S. Klein and J. Nystrand, Phys. Rev. C **60**, 014903 (1999)
  - [36] M. B. Gay Ducati, M. T. Griep and M. V. T. Machado, Phys. Rev. D **88**, 017504 (2013)
  - [37] M. B. G. Ducati, M. T. Griep and M. V. T. Machado, Phys. Rev. C **88**, 014910 (2013)
  - [38] G. M. Yu and Y. D. Li, Chin. Phys. Lett. **30**, 011201 (2013).

- [39] M. Kusek-Gawenda and A. Szczurek, Phys. Rev. C **93**, no. 4, 044912 (2016)
- [40] W. Zha [STAR Collaboration], J. Phys. Conf. Ser. **779**, no. 1, 012039 (2017).
- [41] J. Adam *et al.* [ALICE Collaboration], Phys. Rev. Lett. **116**, no. 22, 222301 (2016)
- [42] X. l. Zhu, P. f. Zhuang and N. Xu, Phys. Lett. B **607**, 107 (2005)
- [43] B. Chen, Phys. Rev. C **93**, no. 4, 044917 (2016)
- [44] Y. p. Liu, Z. Qu, N. Xu and P. f. Zhuang, Phys. Lett. B **678**, 72 (2009); Y. Liu, Z. Qu, N. Xu and P. Zhuang, J. Phys. G **37**, 075110 (2010)
- [45] B. Chen and J. Zhao, Phys. Lett. B **772**, 819 (2017)
- [46] K. J. Eskola, V. J. Kolhinen and C. A. Salgado, Eur. Phys. J. C **9**, 61 (1999)
- [47] B. Chen, T. Guo, Y. Liu and P. Zhuang, Phys. Lett. B **765**, 323 (2017).
- [48] J. Zhao and B. Chen, Phys. Lett. B **776**, 17 (2018)
- [49] R. Aaij *et al.* [LHCb Collaboration], JHEP **1302**, 041 (2013)
- [50] B. Abelev *et al.* [ALICE Collaboration], JHEP **1207**, 191 (2012)
- [51] B. Abelev *et al.* [ALICE Collaboration], JHEP **1209**, 112 (2012)
- [52] B. Abelev *et al.* [ALICE Collaboration], Phys. Rev. Lett. **111**, 102301 (2013)
- [53] M. He, R. J. Fries and R. Rapp, Phys. Rev. C **91**, no. 2, 024904 (2015);
- [54] M. He, R. J. Fries and R. Rapp, Phys. Lett. B **735**, 445 (2014)
- [55] X. Yao and B. Müller, arXiv:1709.03529 [hep-ph].
- [56] B. Chen, Y. Liu, K. Zhou and P. Zhuang, Phys. Lett. B **726**, 725 (2013)
- [57] J. Sollfrank, P. Huovinen, M. Kataja, P. V. Ruuskanen, M. Prakash and R. Venugopalan, Phys. Rev. C **55**, 392 (1997)
- [58] C. Patrignani *et al.* [Particle Data Group], Chin. Phys. C **40**, no. 10, 100001 (2016).
- [59] W. Zha *et al.*, arXiv:1705.01460 [nucl-th].
- [60] M. B. Gay Ducati and S. Martins, Phys. Rev. D **96**, no. 5, 056014 (2017)
- [61] V. Guzey, E. Kryshen and M. Zhalov, Phys. Rev. C **93**, no. 5, 055206 (2016)
- [62] M. Vidovic, M. Greiner, C. Best and G. Soff, Phys. Rev. C **47**, 2308 (1993).
- [63] A. Pautz and G. Shaw, Phys. Rev. C **57**, 2648 (1998)
- [64] J. A. Crittenden, *Exclusive Production of Neutral Vector Mesons at the Electron-Proton Collider HERA (Springer-Verlag, Berlin, 1997)*
- [65] M. G. Ryskin, Z. Phys. C **57**, 89 (1993).
- [66] B. Abelev *et al.* [ALICE Collaboration], Phys. Lett. B **718**, 1273 (2013)
- [67] E. Abbas *et al.* [ALICE Collaboration], Eur. Phys. J. C **73**, no. 11, 2617 (2013)
- [68] V. Pozdniakov *et al.* [ALICE Collaboration], arXiv:1710.03417 [hep-ex]
- [69] G. Sampaio dos Santos and M. V. T. Machado, J. Phys. G **42**, no. 10, 105001 (2015)
- [70] F. Bossu, Z. C. del Valle, A. de Falco, M. Gagliardi, S. Grigoryan and G. Martinez Garcia, arXiv:1103.2394 [nucl-ex].
- [71] X. Zhao and R. Rapp, Phys. Rev. C **82**, 064905 (2010)